Computers and Structures 153 (2015) 19–35

Contents lists available at ScienceDirect

Computers and Structures

journal homepage: www.elsevier.com/locate/compstruc

Adaptive finite element based shape optimization in laminated composite plates

P.M. Mohite *, C.S. Upadhyay

Department of Aerospace Engineering, Indian Institute of Technology Kanpur 208016, India

ARTICLE INFO

Article history:
Received 2 October 2014
Accepted 14 February 2015

Keywords:
Higher order shear deformation model
Strain recovery
a-posteriori error estimation
Discretization error
Shape optimization
First-ply failure

ABSTRACT

In this study a reliable shape optimization for laminated plate structures has been attempted. For a fixed higher order plate model, a simple a-posteriori strain recovery algorithm, following ZZ type patch recovery technique, has been developed. The recovery is seen to be accurate. The effect of higher approximation order and mesh refinement on the quality of the obtained solution quantities like stress components and displacements, is studied in detail. The shape of the cutout is optimized with weight minimization as the objective function and the first-ply failure criterion as the constraint. It is observed that control of the discretization error (via adaptive mesh refinements) leads to vastly different final designs, as compared to those obtained using reasonably refined meshes, but without adaptivity. It is seen that without adaptivity, the design obtained is unsafe, as either more material removal is predicted or failure is predicted at higher loads, as compared to that obtained using adaptivity.

1. Introduction

Composite materials are finding wide applications in critical structural applications due to their capability of giving desired enhanced properties. Moreover, one can tailor these properties according to the requirements. These materials have very high strength to weight ratios. Cutouts in these critical structural components are inevitable. For example, in aerospace applications cutouts are made in wing ribs to facilitate the easy passage of fuel. Sometimes the cutouts are made to provide access for damage inspection or electrical circuits. In aerospace applications, weight saving is one of the important design criteria. Therefore, the cutouts are made just to reduce the weight of the structures. Since, these components are used for critical applications one should have confidence in the design procedure adopted.

A typical optimization based designing procedure involves evaluation of an objective function subjected to one or more constraints. For example, the objective function could be cost or weight minimization or profit maximization. Optimization problems, from engineering discipline, involve evaluation of the constraints which may include state of stress at a point; or a function which is a combination of stress components; deflection at a particular point; thermal stresses; buckling load, etc. Accurate computation of these constraints plays an important role in a reliable optimum design. In engineering design and optimization of large sized critical components, the use of finite element technique has become an integral part. Therefore, accurate evaluation of the finite element data, which in turn, is used in constraint evaluation, is very important.

Many researchers have attempted to optimize the composite laminate with design variables like ply thickness and ply orientation in order to obtain minimum weight designs subjected to several constraints, such as maximum deflection, maximum strength, maximum stress, von-Mises stress, first ply failure load (or reliability requirements), etc. (see [1–4]). The optimum design of laminated plates for maximum buckling load has also been attempted in [5–8] with constraint on the natural frequency. Botkin [9] has worked on shape optimization of stamped sheet metal parts with buckling and stress constraints. Sometimes the cutouts are just unavoidable in laminated structures. Hence, the shape optimization of laminated plates with cutouts for weight minimization has gained importance. For example, one can see the work on the optimization of composite plates with a cutout in [10,11]. Sivakumar et al. [12] have worked on optimization with dynamic constraints.

A survey on structural optimization can be seen in [13,14]. The optimization of aerospace structures with minimum weight objective, subjected to various constraints is reviewed in [15,16].

In general, the focus in all the studies mentioned above has been to demonstrate the effect of optimization on the final design. Thus, a fixed finite element mesh has been used, with a suitable order of approximation, to obtain the results. The effect of the

* Corresponding author. Tel.: +91 512 2596024; fax: +91 512 2597561/7626.
E-mail address: mohite@iitk.ac.in (P.M. Mohite).

http://dx.doi.org/10.1016/j.compstruc.2015.02.020
0045-7949/

discretization error on the final optimal design was not studied. The early work which involves the study of effect of discretization error, on the final optimum shape, was seen due to Kikuchi et al. [17]. In the shape optimization procedure, due to change in shape, the mesh gets distorted and the final design is sensitive to the approximation error associated with the discretization. Thus, improvement in the quality of the approximation is needed [17]. In this work global error estimates were developed for adaptive refinement strategies. A similar work was carried out by Hinton et al. [18]. Weck et al. [19] have worked on saving the computational cost during optimization of composite structures with ply-orientations and thickness as optimization variables using adaptive meshing technique. Benneet and Botkin [20] aimed to provide more accurate estimate of the true optimal solution with the effect of adaptive meshing on stresses used in constraint evaluation. Schleupen et al. [21] developed both global (based on error of the strain energy of overall structure) and local error estimates (based on error in a particular quantity of interest like displacement or stress component) for global and local adaptive refinements separately. The potential of these two techniques were then compared through two dimensional shape optimization problems. Morin et al. [22] developed an algorithm based on adaptive finite element method to equidistribute the errors due to shape optimization and discretization to optimize the computational cost. An application to X-FEM based structural optimization can be seen in [23]. An evolutionary technique was used along with sensitivity analysis, for a low cost adaptive remeshing, in shape optimization problems by Bugeda et al. [24].

The application of adaptive meshing using goal oriented error control for topology optimization was done by Bruggi and Verani [25]. Another application of adaptive refinement approach to topology optimization can be seen in Wang et al. [26].

In the present work a design of laminated composite plate, with a centrally located cutout for minimum weight, subjected to a constraint that the plate should not fail under first-ply failure load criterion, has been studied. Here, an attempt is made to demonstrate the effect of reliability of constraints on the final optimal solution. Initially, the final optimal solution is obtained without considering reliability of the computed data used in the evaluation of first-ply failure load constraint. The process is then repeated with a control on the reliability of the computed data, i.e. effect of discretization error control on final optimal shape. In the present work a higher order shear deformable plate theory proposed by Reddy [27] has been adopted and implemented in a finite element code. Further, Zienkiewicz-Zhu (ZZ) [28–31] type a-posteriori patch recovery based error estimator is developed for strain field corresponding to the plate model considered. Although, the use of Genetic Algorithms (GA) (for example, [12]) and evolutionary algorithms (for example [24]) is very popular in optimization studies, in the present study we have used a conventional optimization algorithm - Complex Search [32] to obtain an optimal design. Finally, the effect of evaluation of first-ply failure load constraint, with and without control in discretization error, is studied. Here, the Tsai-Wu first-ply failure criterion [33] has been used as a constraint.

2. Problem formulation

In this section a higher order shear deformable plate theory due to Reddy [27] is presented followed by the finite element formulation for this plate model.

2.1. Higher order plate model

Symmetric laminates find many applications in the aircraft industry. Although symmetric laminates are simple to analyze and design, some specific applications of laminated composites require unsymmetric laminates. For example, the coupling between bending and extension exhibited by this type of laminates is an essential feature of jet turbine fan blades with pre-twist. It can be noted that the theories for unsymmetric laminates are applicable to symmetric laminates as a special case. Unlike symmetric laminates, unsymmetric laminates exhibit membrane-flexure coupling phenomenon, which necessitates the use of a displacement field containing both, membrane as well as flexure deformation terms which contribute to the overall response of a laminate. The analysis of laminated plates is based on the choice of a plate theory. Several plate theories have been developed with assumed variation of the displacement field in the transverse direction. For example, see plate theories in [3,4,12,34–38]. These theories attempt to give a higher order representation of strains in the laminate thickness direction. In the following, we present the details of plate theory due to Reddy [27] implemented in the present study. The displacement field

$$\mathbf{u}(x,y,z) = [u(x,y,z)\; v(x,y,z)\; w(x,y,z)]^T \tag{1}$$

is derived from the expanded Taylor's series in terms of thickness coordinate z. Here, $u(x,y,z)$, $v(x,y,z)$ and $w(x,y,z)$ are the displacement components along x,y and z axes, respectively. These components, following the work of Reddy [27], are given as

$$\begin{aligned} u(x,y,z) &= u_0(x,y) + z\theta_x(x,y) + z^2\phi_x(x,y) + z^3\psi_x(x,y) \\ v(x,y,z) &= v_0(x,y) + z\theta_y(x,y) + z^2\phi_y(x,y) + z^3\psi_y(x,y) \\ w(x,y,z) &= w_0(x,y) \end{aligned} \tag{2}$$

In the expansion in Eq. (2), it is assumed that transverse normal strain ϵ_{zz} is zero. The linear strain–displacement relationships using small deformation theory can be obtained from this equation.

The condition that the transverse shear stresses vanish on the plate's top and bottom faces (see Fig. 1) is equivalent to the requirement that the corresponding strains be zero on these surfaces, i.e.

$$\gamma_{yz}\left(x,y,\pm\frac{d}{2}\right) = \gamma_{xz}\left(x,y,\pm\frac{d}{2}\right) = 0 \tag{3}$$

On introduction of these conditions in the expressions for transverse shear strains, the following relations are obtained.

$$\phi_x = \phi_y = 0; \quad \psi_y = -\frac{4}{3d^2}(\theta_y + w_{0,y}) \quad \text{and} \quad \psi_x = -\frac{4}{3d^2}(\theta_x + w_{0,x}) \tag{4}$$

The displacement field of Eq. (2) is modified by setting ϕ_x and ϕ_y to be zero according to conditions of Eq. (4). The resulting displacement field is now written as

$$\begin{aligned} u(x,y,z) &= u_0(x,y) + z\,\theta_x(x,y) + z^3\,\psi_x(x,y) \\ v(x,y,z) &= v_0(x,y) + z\,\theta_y(x,y) + z^3\,\psi_y(x,y) \\ w(x,y,z) &= w_0(x,y) \end{aligned} \tag{5}$$

In Eq. (5) u_0, v_0 and w_0 are the mid-plane displacement components while θ_x and θ_y are the rotations about y and x axes, respectively. Further, ψ_x and ψ_y are higher order terms in the Taylor's series expansion and are also defined at the mid-plane. Thus, the generalized displacement vector $\{\delta\}$ of the mid-surface contains seven degrees of freedom (DOF) and is given by:

$$\{\delta\} = \{u_0\; v_0\; w_0\; \theta_x\; \theta_y\; \psi_x\; \psi_y\}^T \tag{6}$$

The corresponding strain–displacement relations, using infinitesimal strains, are:

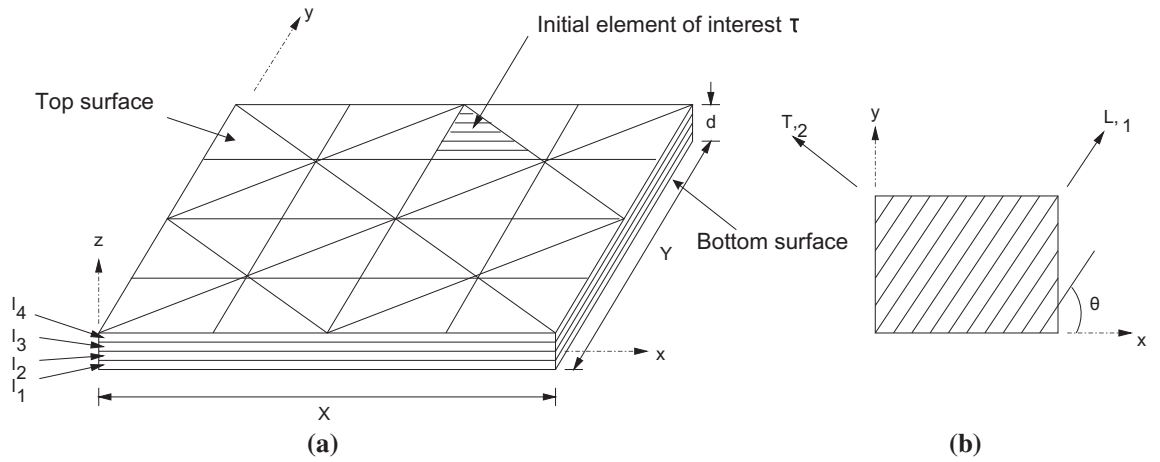

Fig. 1. Laminate geometry, coordinate systems, stacking sequence and layer numbering.

$$
\begin{aligned}
\epsilon_{xx} &= u_{0,x} + z\,\theta_{x,x} + z^3\,\psi_{x,x} \\
\epsilon_{yy} &= v_{0,y} + z\,\theta_{y,y} + z^3\,\psi_{y,y} \\
\gamma_{xy} &= u_{0,y} + v_{0,x} + z\,\theta_{x,y} + z\,\theta_{y,x} + z^3\,\psi_{x,y} + z^3\,\psi_{y,x} \\
\gamma_{yz} &= \theta_y + 3\,z^2\,\psi_y + w_{0,y} \\
\gamma_{xz} &= \theta_x + 3\,z^2\,\psi_x + w_{0,x}
\end{aligned}
\tag{7}
$$

Here, comma $(,)$ denotes the partial derivative.

2.2. Finite element formulation

The total potential, Π_p, for the structure is given by

$$
\Pi_p(\mathbf{u}) = \frac{1}{2}\int_V \boldsymbol{\sigma}(\mathbf{u})\cdot\boldsymbol{\varepsilon}(\mathbf{u})\,dV - \int_{R^+\cup R^-} T_3\,u_3\,ds - \int_{\Gamma_N} (T_1\,u_1 + T_2\,u_2)\,ds \tag{8}
$$

where V is the volume enclosed by the plate domain; $\boldsymbol{\sigma}(\mathbf{u})$ and $\boldsymbol{\varepsilon}(\mathbf{u})$ are the engineering stress and strain vectors, respectively. R^+ and R^- denote the top and bottom faces of the laminated plate and $T_3(x,y)$ is the applied transverse load on these faces; Γ are the lateral faces with $\Gamma = \Gamma_N \cup \Gamma_D$. Here, Γ_N denotes the Neumann boundary and Γ_D denotes Dirichlet boundary; T_1, T_2 are the in-plane tractions specified on the lateral faces along 1 and 2 directions, respectively. Here, u_1, u_2 and u_3 denote the three components of the displacement field $\mathbf{u}$ in 1, 2 and 3 directions, respectively. Using the model described by (5), the total potential $\Pi(\mathbf{u})$ can be defined by substituting $\mathbf{u}$ in Eq. (8).

The approximate solution to the problem, $\mathbf{u}^h$, is the minimizer of the total potential $\Pi_p(\mathbf{u}^h)$ and is obtained from the solution of the following weak problem:

Find $\mathbf{u}^h \in H^0(\mathbf{V})$ such that

$$
\mathcal{B}(\mathbf{u}^h, \mathbf{v}^h) = \mathcal{F}(\mathbf{v}^h) \quad \forall\ \mathbf{v}^h\ H^0(\mathbf{V}) \tag{9}
$$

where

$$
\mathcal{B}(\mathbf{u}^h, \mathbf{v}^h) = \int_V \{\boldsymbol{\sigma}(\mathbf{u}^h)\}^T \{\boldsymbol{\varepsilon}(\mathbf{v}^h)\}\,dV, \tag{10}
$$

$$
\mathcal{F}(\mathbf{v}^h) = -\int_{R^+\cup R^-} T_3\,v_3^h\,ds - \int_{\Gamma_N} (T_1\,v_1^h + T_2\,v_2^h)\,ds \tag{11}
$$

and $H^0(\mathbf{V}) = \{\mathbf{v}^h \mid \Pi_p(\mathbf{v}^h) < \infty \text{ and } \mathcal{M}\mathbf{v}^h = \mathbf{0} \text{ on } \Gamma_D\}$; $\mathbf{v}^h$ is the test function and has the same form as $\mathbf{u}^h$ given by (2). We will further define $\sqrt{\mathcal{B}(\mathbf{v},\mathbf{v})} = \|\mathbf{v}\|_E$ as the energy norm. Note that $\mathcal{B}(\mathbf{u}^h, \mathbf{u}^h) = 2\mathcal{U}(\mathbf{u}^h)$ where $\mathcal{U}(\mathbf{u}^h)$ is the strain energy for the solution $\mathbf{u}^h$. Note that in this study Dirichlet means the part of lateral boundary where geometric constraints are imposed, while Neumann stands for the parts of the lateral boundary where in-plane traction is applied. Further, $\mathcal{M}$ is a generic representation of displacement constraints on the Dirichlet boundary edge. For example, the boundary conditions can be clamped $(u_i = 0, i = 1,2,3)$; soft simple-support $(u_n, u_3 = 0)$; hard simple-support $(u_t, u_3 = 0)$; etc. Here, u_n and u_t denote in-plane displacement components normal and tangential to an edge, respectively.

Triangular elements are used in the finite element approximation employed in this study, along with hierarchic shape functions of order p $(p \leqslant 4)$. The mesh generation is done using advancing front method based automatic mesh generator. A typical mesh generated over the plate domain is shown in Fig. 2.

A detailed study on various plate models for laminate applications and their finite element implementation can be seen in Pandya and Kant [36–38].

3. A-posteriori recovery of pointwise strains and error estimation

In a typical engineering analysis a mathematical model for physical problem is first selected, such that it incorporates the essential features of the actual physical problem. The finite element method determines an approximation to the exact solution of the mathematical model. The computed solution should be compared with exact solution of the mathematical model which is being solved. Hence, the computed results can be used to make engineering decisions only when one can guarantee that finite

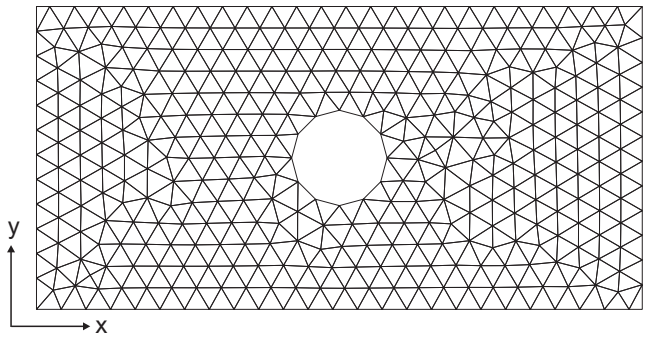

Fig. 2. Rectangular domain with a circular cutout, meshed with an advancing front method based automatic mesh generator.

element solution is sufficiently close to the exact solution of the mathematical model problem. In general, the results of interest obtained from the finite element solution can be very different from those corresponding to the exact solution of the mathematical formulation and can lead to serious design errors. Thus, it is imperative to accompany any computational analysis with an accurate indication of the error in the quantity of interest.

The error estimator should be reliable. Unreliable error estimates are dangerous because they could lead to a misleading confidence in the computed quantities. The reliability of the error estimator has to be understood with respect to the solution quantity of interest. Here, an error estimator is constructed for the energy norm of the error and it is assumed that if the error in the global energy norm is low then all solution quantities of interest are also reasonably accurate.

Many classes of a-posteriori error estimators are available in the literature (see [39–41]). For the three-dimensional problems, the implicit type residual error estimators would prove to be computationally expensive. Hence, the more economical recovery (or projection) based error estimators have been employed in this study. It was found in [42,43] that the error estimator based on stress recovery (defined in [29]) was reliable locally for patches at the boundary of the domain, as well as the interior of the domain. Several definitions of such projections are possible (see [42,44]).

In this study a simple procedure for the recovery of strains, from the finite element solution, using patchwise data is proposed (as an extension of the method in [45]). More details of this estimator can be seen in earlier works of authors [46,47]. These recovered strains will be then used to design a simple error estimator.

3.1. Procedure for recovery of strains

Following the representation of the solution by Eq. (7), we re-write the components of strain in the following form as

$$\boldsymbol{\epsilon} = \begin{Bmatrix} \varepsilon_{xx} \\ \varepsilon_{yy} \\ \gamma_{yz} \\ \gamma_{xz} \\ \gamma_{xy} \end{Bmatrix} = \begin{Bmatrix} \varepsilon_{xx}^{(0)} \\ \varepsilon_{yy}^{(0)} \\ \gamma_{yz}^{(0)} \\ \gamma_{xz}^{(0)} \\ \gamma_{xy}^{(0)} \end{Bmatrix} + z \begin{Bmatrix} \varepsilon_{xx}^{(1)} \\ \varepsilon_{yy}^{(1)} \\ 0 \\ 0 \\ \gamma_{xy}^{(1)} \end{Bmatrix} + z^2 \begin{Bmatrix} 0 \\ 0 \\ \gamma_{yz}^{(1)} \\ \gamma_{xz}^{(1)} \\ 0 \end{Bmatrix} + z^3 \begin{Bmatrix} \varepsilon_{xx}^{(2)} \\ \varepsilon_{yy}^{(2)} \\ 0 \\ 0 \\ \gamma_{xy}^{(2)} \end{Bmatrix} \tag{12}$$

The recovered strain $\boldsymbol{\epsilon}^*$ is also assumed to have the same form (in terms of z) as the exact one, Eq. (7). Thus, the recovered strain is also represented as

$$\boldsymbol{\epsilon}^* = \begin{Bmatrix} \varepsilon_{xx}^* \\ \varepsilon_{yy}^* \\ \gamma_{yz}^* \\ \gamma_{xz}^* \\ \gamma_{xy}^* \end{Bmatrix} = \begin{Bmatrix} \varepsilon_{xx}^{*,(0)} \\ \varepsilon_{yy}^{*,(0)} \\ \gamma_{yz}^{*,(0)} \\ \gamma_{xz}^{*,(0)} \\ \gamma_{xy}^{*,(0)} \end{Bmatrix} + z \begin{Bmatrix} \varepsilon_{xx}^{*,(1)} \\ \varepsilon_{yy}^{*,(1)} \\ 0 \\ 0 \\ \gamma_{xy}^{*,(1)} \end{Bmatrix} + z^2 \begin{Bmatrix} 0 \\ 0 \\ \gamma_{yz}^{*,(1)} \\ \gamma_{xz}^{*,(1)} \\ 0 \end{Bmatrix} + z^3 \begin{Bmatrix} \varepsilon_{xx}^{*,(2)} \\ \varepsilon_{yy}^{*,(2)} \\ 0 \\ 0 \\ \gamma_{xy}^{*,(2)} \end{Bmatrix} \tag{13}$$

Given the representation of $\boldsymbol{\epsilon}^*$ as in Eq. (13), it is now desired to obtain the recovered strain field as a polynomial, element by element, such that the recovered strain components are polynomials that are one order higher than the corresponding finite element strain components. Thus, if the order of approximation for elements p is employed then all the recovered in-plane strain components will be polynomials of degree p and the out of plane strain components will be polynomials of degree $(p+1)$. The representation of the recovered strain components in terms of polynomials are given below. For example, $\epsilon_{xx}^{*(0)}$ is given as

$$\epsilon_{xx}^{*(0)} = \sum_{i=1}^{(p+1)(p+2)/2} e_{xx,i}^{*(0)}\, q_i \tag{14}$$

where $e_{xx,i}^{*(0)}$ denotes the unknown coefficients and q_i are the monomials. The monomials are defined in terms of a local coordinate system described later. Similarly, the strain components $\epsilon_{xx}^{*(1)}, \epsilon_{xx}^{*(2)}, \epsilon_{yy}^{*0}, \epsilon_{yy}^{*(1)}, \epsilon_{yy}^{*(2)}, \epsilon_{xy}^{*(0)}, \epsilon_{xy}^{*(1)}$ and $\epsilon_{xy}^{*(2)}$ can be approximated as above.

Now, the transverse shear strain components of the strain tensor are approximated by $(p+1)$th order polynomial. For example,

$$\gamma_{yz}^{*(0)} = \sum_{i=1}^{(p+2)(p+3)/2} e_{yz,i}^{*(0)}\, q_i \tag{15}$$

Similarly, the strain components $\gamma_{yz}^{*(1)}, \gamma_{xz}^{*(0)}$ and $\gamma_{xz}^{*(1)}$ can be approximated as above.

A patch is constructed by taking an element τ and one layer neighborhood of elements around it, as shown in Fig. 3. Let the centroid of the element τ be (x_c, y_c). A local coordinate system can be defined, with x_c and y_c as the center, as

$$\begin{Bmatrix} \hat{x} \\ \hat{y} \end{Bmatrix} = \begin{Bmatrix} x - x_c \\ y - y_c \end{Bmatrix} \tag{16}$$

The monomials q_i are given as,

$$q_1 = 1, q_2 = \hat{x}, q_3 = \hat{y}, q_4 = \hat{x}^2, q_5 = \hat{x}\hat{y}, q_6 = \hat{y}^2, \ldots \tag{17}$$

Now, to recover a smoothened strain field we should find smoothened strain components. To get these coefficients, as aforesaid, the strain recovery procedure uses the principle of minimization of energy norm of the error, i.e. the energy due to errors in strain and stress components, over the patch considered. A typical patch, with a layer of one element neighborhood, over element τ is shown in Fig. 3. In this, the strain components of the finite element solution are known. The material properties and other relevant information about patch is also available. From this, the strain energy of the error can be computed as,

$$J = \frac{1}{2} \int_{A_{patch}} \int_{z=-\frac{d}{2}}^{\frac{d}{2}} \left(\boldsymbol{\epsilon}^* - \boldsymbol{\epsilon}^h\right) \cdot \overline{\mathbf{Q}} \left(\boldsymbol{\epsilon}^* - \boldsymbol{\epsilon}^h\right) dz\, dA \tag{18}$$

where $\boldsymbol{\epsilon}^*$ and $\boldsymbol{\epsilon}^h$ are the recovered and finite element strain vectors and $\overline{\mathbf{Q}}$ is material stiffness matrix, respectively. Note that J is the strain energy of the error in the strain, $\boldsymbol{\epsilon}^* - \boldsymbol{\epsilon}^h$. In Eq. (18), although, the material stiffness matrix $\overline{\mathbf{Q}}$ varies over the laminate thickness, it is constant over a given lamina thickness. Hence, the integration over laminate thickness can be written as sum of integration over the individual lamina thicknesses. Further, the integration over patch area can be written as sum of integration over the element areas in the patch. Thus, the above equation can be written as

$$J = \frac{1}{2} \sum_{i=0}^{N_P - 1} \int_{\tau_i^p} \left[\sum_{l=1}^{NLAY} \int_{z_{l-1}}^{z_l} \left\{ \left(\boldsymbol{\epsilon}^* - \boldsymbol{\epsilon}^h\right) \cdot \overline{\mathbf{Q}}^{(l)} \left(\boldsymbol{\epsilon}^* - \boldsymbol{\epsilon}^h\right) \right\} dz \right] dA \tag{19}$$

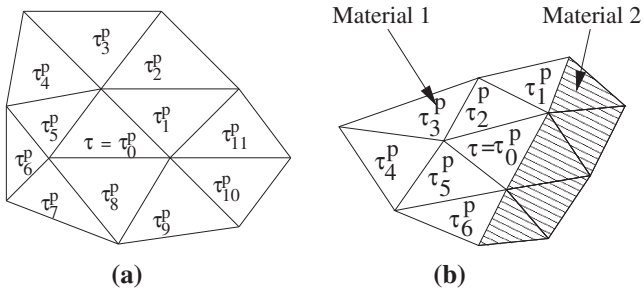

Fig. 3. One element neighborhood patch P_τ over an element τ consisting of elements (a) $\left\{\tau_j^{(p)}\right\}, j = 0, 1, 2, \ldots, 11$ in one material and (b) $\left\{\tau_j^{(p)}\right\}, j = 0, 1, 2, \ldots, 6$ in two different materials.

where N_P is the number of elements in the patch over an element τ, *NLAY* is the number of laminae in the laminate, $\overline{\mathbf{Q}}^{(l)}$ is the material stiffness matrix and z_l and z_{l-1} are the top and bottom coordinates of lth lamina, respectively.

The minimization of the function J with respect to each unknown coefficient of recovered strain term gives as many linearly independent equations as the number of coefficients in Eq. (18). The coefficients are solved for each element patch and the values are retained for the element τ.

The above step is followed by 'reconstruction'. In this, using these coefficients, smoothened strain components can be constructed over the patch. These strains, in turn, can be used to construct the stress components. The in-plane stresses are constructed using material properties, i.e. from the constitutive equation. Although, the recovered shear strains are improvements over the finite element strains, equilibrium equations are used to get the transverse stress field as the model used itself will not give good transverse stress components. This is because the strain continuity through the laminate thickness has been assumed and it will lead to discontinuity of stresses at the interfaces.

The strain energy from recovered and finite element strains are calculated over the whole domain.

$$\begin{aligned} \mathcal{U}^* &= \frac{1}{2}\sum_{j=1}^{NEL}\int_j \boldsymbol{\sigma}^* \cdot \boldsymbol{\epsilon}^*\, dV_{patch} \\ \mathcal{U}^h &= \frac{1}{2}\sum_{j=1}^{NEL}\int_j \boldsymbol{\sigma}^h \cdot \boldsymbol{\epsilon}^h\, dV_{patch} \end{aligned} \tag{20}$$

where $\mathcal{U}^*$ and $\mathcal{U}^h$ are the strain energies over the whole domain from recovered strains and finite element strains, respectively. $\boldsymbol{\sigma}^*$ and $\boldsymbol{\sigma}^h$ are the recovered and finite element stresses, $\boldsymbol{\epsilon}^*$ and $\boldsymbol{\epsilon}^h$ are the recovered and finite element strains, respectively and *NEL* is the number of elements in the mesh constructed over the domain.

Remark: When there is a material discontinuity, the averaging is done over the elements with same material. For example, given the element τ_0^p, the patch consists of elements $\{\tau_i^p\} i = 0, 1, \ldots, 6$ (see Fig. 3(b)).

Remark: No attempt is made here to obtain a smoothened stress or strain field (as prescribed in [30,31]). It is expected, following the work of [42,45], that the recovered strain field will be more accurate than that obtained by the finite element solution.

4. Definition of a-posteriori error estimator based on strain recovery

The recovered strain $\boldsymbol{\epsilon}^*$ can be used to define an a-posteriori estimate of the error. The element error indicator η_τ, for an element τ is given as:

$$\eta_\tau^2 = \int_\tau \left[\sum_{i=1}^{NLAY}\int_{z_{i-1}}^{z_i} \left\{(\boldsymbol{\epsilon}^* - \boldsymbol{\epsilon}^h)\cdot \overline{\mathbf{Q}}^i (\boldsymbol{\epsilon}^* - \boldsymbol{\epsilon}^h)\right\} dz\right] dA \tag{21}$$

The element error indicators can be used to define the global error estimator ξ_Ω as:

$$\xi_\Omega = \sqrt{\sum_{\tau=1}^{NEL}\eta_\tau^2} \tag{22}$$

The error estimator based on the recovered strain developed above has to be tested for robustness and accuracy. Following the work of [42,45], it is imperative to subject an estimator to rigorous bench-marking tests in order to ascertain the quality of the estimator for the class of materials, domains, loading and boundary conditions of interest. In [44,45], a rigorous mathematical proof was given, which leads to a simple computer-based procedure for testing the quality of a-posteriori error estimators for general second order elliptic problems. A detailed study was carried out by the authors in [46] to ascertain the quality of the estimator. The procedure was based on the basic idea given in [44]. The procedure is presented in the following for the sake of completeness. For more details, see the earlier work of authors in [46].

Let $\bar{\omega}$ be a small subregion of interest, lying inside the domain Ω. Then asymptotically, for $\bar{\omega}$ sufficiently small, the finite element solution is essentially the best approximation of the local $(p+1)$th order Taylor series expansion of the exact solution $\mathbf{u}$, over a region slightly bigger than $\bar{\omega}$. It was assumed for the asymptotic error analysis that all global contributions to error in the local region $\bar{\omega}$ (i.e. pollution error) were negligible. Further, it was assumed that the dominant part of the local error was due to the $(p+1)$th degree terms of the local Taylor series expansion of the exact solution.

However, for laminated composite plates, limited detailed interior analysis of local error exists (for example see the earlier works of authors in [46–50]). In [46], the work of [51,52] was followed to get the global component of the error (for a rectangular plate) in a local region $\bar{\omega}$ due to only boundary layer effect. The effect of the thickness of the plate, d, on the convergence rate is seen through a slowing down in the setting of asymptotic behavior, i.e. a more refined mesh may be required to get asymptotic behavior. This phenomenon is also known as locking effect. It is known that the h-version of the finite element method can be used to control the boundary layer effect by using sufficient mesh refinements near the boundaries. Assuming that the thickness d is fixed (away from zero), for the error $\mathbf{e} = \mathbf{u} - \mathbf{u}^h$, we can write

$$||\mathbf{e}||_{E(\Omega)} \leqslant C(d)\, h^{\mu} \tag{23}$$

where $\mu = \min(p, r)$ and r depends on the regularity of the solution $\mathbf{u}$ of the plate model; $\|\cdot\|_{E(\bar{\omega})}$ is the energy norm given by $\|\mathbf{u}\|_{E(\bar{\omega})} = \sqrt{2\,\mathcal{U}_{\bar{\omega}}(\mathbf{u})}$. Here, $\mathcal{U}_{\bar{\omega}}$ is the strain energy of $\mathbf{u}$ over region $\bar{\omega}$.

Further, assume that for a subregion $(\bar{\omega}) \in \Omega$, sufficiently away from the boundary

$$||\mathbf{e}||_{E(\bar{\omega})} \leqslant C(d)\, h^{p} \tag{24}$$

in the absence of boundary layer effects, and for a fixed d. The readers are referred to the work of [53] for a detailed proof on convergence of local error for isotropic plates. Thus, if the finite element solution is obtained over the same mesh using $(p+1)$ order elements, the error $\mathbf{e}^{(p+1)} = \mathbf{u} - \mathbf{u}_{FE}^{(p+1)}$ in the finite element solution $\mathbf{u}_{FE}^{(p+1)}$ satisfies

$$||\mathbf{e}^{(p+1)}||_{E(\bar{\omega})} \leqslant C(d)\, h^{(p+1)} \tag{25}$$

Hence, we can obtain,

$$\begin{aligned} ||\mathbf{e}||_{E(\bar{\omega})} &= ||\mathbf{u} - \mathbf{u}_{FE}^{(p+1)} + \mathbf{u}_{FE}^{(p+1)} - \mathbf{u}^h||_{E(\bar{\omega})} \leqslant ||\mathbf{u} - \mathbf{u}_{FE}^{(p+1)}||_{E(\bar{\omega})} \\ &+ ||\mathbf{u}_{FE}^{(p+1)} - \mathbf{u}^h||_{E(\bar{\omega})} \approx ||\mathbf{u}_{FE}^{(p+1)} - \mathbf{u}^h||_{E(\bar{\omega})} \end{aligned} \tag{26}$$

thus, Eq. (26) means that the error is essentially the difference between the $(p+1)$th order solution and the pth order solution, when $h \to 0$. Here it is to be noted that $\mathbf{u}_{FE}^{(p+1)}$ denotes the finite element solution $\mathbf{u}^h$ obtained with an approximation of order $(p+1)$.

Letting $\xi_{\bar{\omega}}$ be the error estimator for subregion $\bar{\omega}$, we define

$$\kappa_{\bar{\omega}} = \frac{\xi_{\bar{\omega}}}{||\mathbf{e}||_{E(\bar{\omega})}} \approx \frac{\xi_{\bar{\omega}}}{||\mathbf{u}_{FE}^{(p+1)} - \mathbf{u}^h||_{E(\bar{\omega})}} \tag{27}$$

where $\kappa_{\bar{\omega}}$ is the effectivity index for the subregion $\bar{\omega}$. Ideally, $\kappa_{\bar{\omega}} = 1$ is desired.

The details of this work for laminated plates with various stacking sequences, boundary conditions, plate length to thickness ratios, materials, mesh patterns, etc. can be seen in earlier work of authors [46]. The quality of the proposed error estimator was also studied in [46].

4.1. Adaptivity

The energy norm of the error obtained using the recovered strain field is used to refine the mesh. The procedure developed is very simple. It involves the computation of the energy norm of the error in each element, followed by a ranking of the elements in the order of highest contributions to the total error. The elements contributing eighty percent or more of the maximum error are refined. This procedure is repeated till convergence to within the specified tolerances is obtained. It should be noted that adaptive analysis requires repeated solution of the boundary value problem, with the modified meshes. Thus, the cost of computation increases (see [39,45] for details).

5. Optimization problem formulation

The plate with dimensions of X, Y, thickness d and a centrally located cutout of elliptical shape with initial size $2a, 2b$ and oriented at θ degrees with respect to x axis, is shown in Fig. 4. Here, $2a$ is major axis, $2b$ is minor axis.

The objective of the optimization problem is to minimize the weight of the plate. Since all the laminae of same material are taken, the objective becomes the minimization of the plate material area. Hence, the design parameters are, semi-major axis - a, semi-minor axis – b and orientation of the elliptical cutout.

$$\begin{aligned}&\textbf{Objective function}: \quad \text{Minimize} \quad \text{weight of the material, } W\\ &\text{Or}\\ &\qquad \text{Minimize} \quad \text{area of the material, } A = XY - \pi ab\\ &\textbf{Subject to}: \quad \text{State of stress is such that the Tsai Wu failure index} \leqslant 0.8 \text{ and}\\ &\qquad \frac{Y}{8} \leqslant a, b \leqslant 0.4Y\end{aligned} \tag{28}$$

The second constraint given above is purely from geometric constraints point of view.

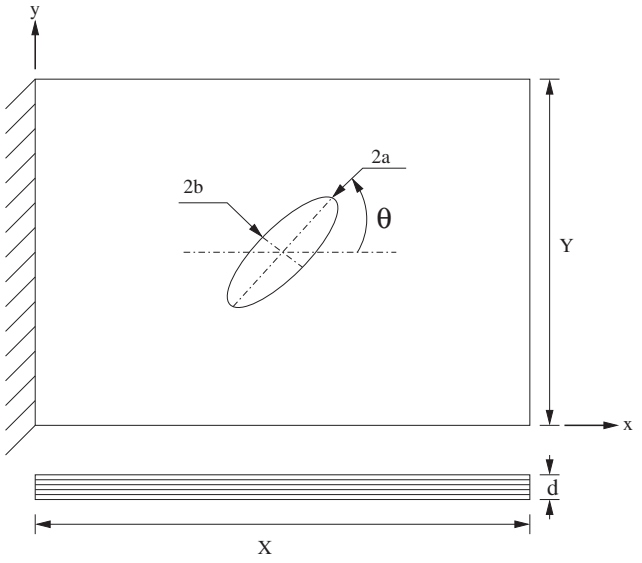

Fig. 4. Geometry of the laminate and initial shape of the cutout.

5.1. Optimization algorithm

Complex Search Method algorithm is used for solving this optimization problem [32]. The algorithm begins with a number of feasible points created at random. If a point is found to be infeasible, a new point is created using previously generated points. Usually, the infeasible point is pushed towards the centroid of the previously found feasible points. Once a set of feasible points is found, the worst point is reflected about the centroid of rest of the points to find a new point. Depending on the feasibility and function value of the new point, the point is further modified or accepted. If the new point falls outside the variable boundaries, the point is modified to fall on the violated boundary. If new point is infeasible, the point is retracted towards the feasible points. The worst point in the simplex is replaced by this new feasible point and algorithm continues for next iteration. Here, the reflection parameter and convergence parameter are chosen as 1.3 and 0.01, respectively.

The algorithm given above is presented in the following.

Step 1: Assume a bound in $x\left(x^{(L)}, x^{(U)}\right)$, a reflection parameter α and termination parameters ϵ and δ.
Strep 2: Generate an initial set of P feasible points
For $p = 1, \ldots, P-1$.

(a) Randomly generate $x_i^{(p)}, i = 1, \ldots, N$

(b) If $x_i^{(p)}$ is infeasible then reset

$$x^{(p)} = x^{(p)} + \frac{1}{2}\left(\bar{x} - x^{(p)}\right) \tag{29}$$

where $\bar{x}$ is the centroid of previously generated feasible points. Repeat this process until $x^{(p)}$ becomes feasible.

(c) Else if $x^{(p)}$ is feasible then continue with (a) until P feasible points are generated.

(d) For all feasible points evaluate the function value $f\left(x^{(p)}\right)$
Set the iteration counter $k = 1$.

Step 3: Reflection step

(a) Select the point x^R such that

$$f\left(x^R\right) = \text{Max } f\left(x^{(p)}\right) = \mathrm{F}_{max} \tag{30}$$

(b) Calculate the centroid $\bar{x}$ of all feasible points except x^R and the new point

$$x^m = \bar{x} + \alpha\left(\bar{x} - x^R\right) \tag{31}$$

(c) If x^m is feasible and $f(x^m) \geqslant \mathrm{F}_{max}$, retract half the distance to the centroid $\bar{x}$. Continue until $f(x^m) < \mathrm{F}_{max}$;

Else if x^m is feasible and $f(x^m) < \mathrm{F}_{max}$, go to Step 5.
Else if x^m is infeasible, go to Step 4.

Step 4: Check for feasibility of the solution

(a) For all i reset violated variable bounds:

$$\begin{aligned}&\text{If} \quad x_i^m < x_i^{(L)} \quad \text{set } x_i^m = x_i^{(L)}\\ &\text{If} \quad x_i^m < x_i^{(U)} \quad \text{set } x_i^m = x_i^{(U)}\end{aligned} \tag{32}$$

(b) If the resulting x^m is infeasible, retract half the distance to the centroid. Continue until x^m is feasible. Go to Step 3(c).

Step 5: Replace x^R by x^m. Check for termination.

(a) Calculate $\bar{f} = \frac{1}{P}\sum_p f\left(x^{(p)}\right)$ and $\bar{x} = \frac{1}{P}\sum_p x^{(p)}$

(b) If $\sqrt{\sum_p \left(f\left(x^{(p)}\right) - \bar{f}\right)^2} \leqslant \epsilon$ and $\sqrt{\sum_p \| x^{(p)} - \bar{x} \|^2} \leqslant \delta$

Terminate;
Else go for another iteration. Set $k = k + 1$ and go to Step 3(a).

5.2. Failure criterion

The failure criterion based on interactive failure theories is considered. We have used here second-order tensor polynomial

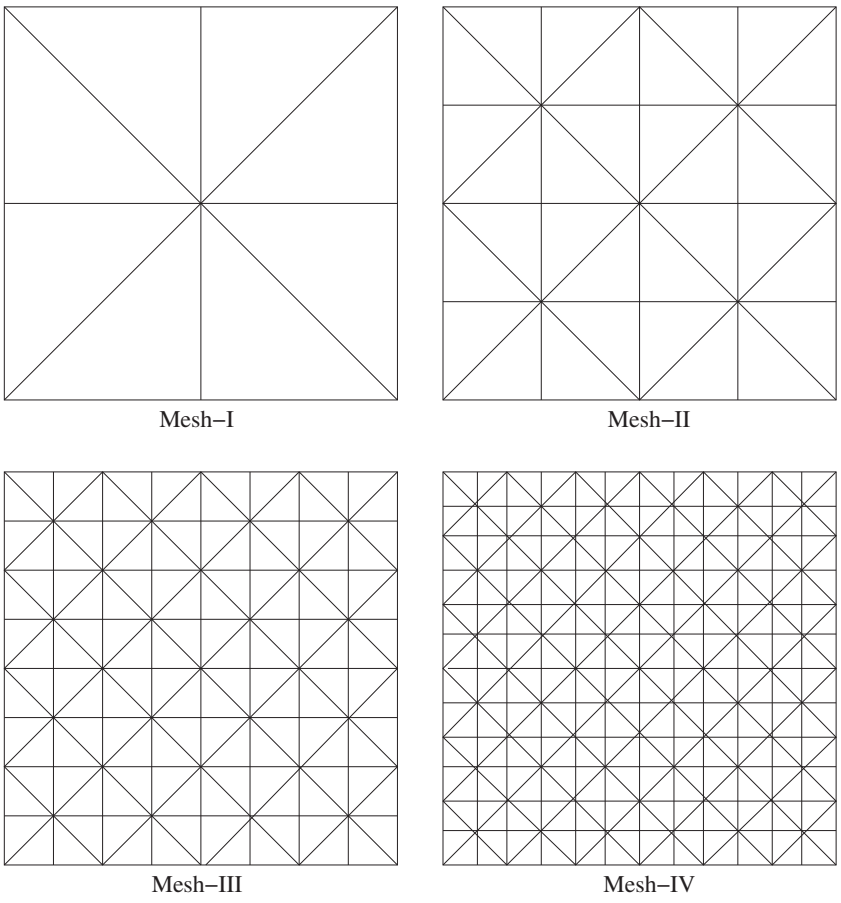

Fig. 5. Mesh types or patterns used for plate validation study.

criterion proposed by Tsai-Wu [33]. It is a complete quadratic tensor polynomial with the linear terms included. The most compact form for expressing this theory is through tensor notation:

$$F_i\,\sigma_i + F_{ij}\,\sigma_i\,\sigma_j \leqslant 0.8 \quad i,j = 1,2,\ldots,6 \tag{33}$$

where F_i and F_{ij} are the strengths tensors established through experimental procedures and are related to failure strengths in principal lamina directions. σ_i denotes the stress components. Here, right hand side of above equation is deliberately taken 0.8 instead of 1 as a safe constraint for the optimization problem mentioned earlier. For orthotropic lamina this reduces to (see [33,54,55] and references therein)

$$\begin{aligned} &F_1\,\sigma_{11} + F_2\,\sigma_{22} + F_3\,\sigma_{33} + F_{11}\,\sigma_{11}^2 + F_{22}\,\sigma_{22}^2 + F_{33}\,\sigma_{33}^2 + F_{44}\,\sigma_{23}^2 + F_{55}\,\sigma_{13}^2 \\ &+ F_{66}\,\sigma_{12}^2 + 2F_{12}\,\sigma_{11}\,\sigma_{22} + 2F_{13}\,\sigma_{11}\,\sigma_{33} + 2F_{23}\,\sigma_{22}\,\sigma_{33} \leqslant 0.8 \end{aligned} \tag{34}$$

The components of the strength tensor are given below as:

$$\begin{aligned} &F_1 = \tfrac{1}{X_T} - \tfrac{1}{X_C}, && F_2 = \tfrac{1}{Y_T} - \tfrac{1}{Y_C}, && F_3 = \tfrac{1}{Z_T} - \tfrac{1}{Z_C}, \\ &F_{11} = \tfrac{1}{X_T X_C}, && F_{22} = \tfrac{1}{Y_T Y_C}, && F_{33} = \tfrac{1}{Z_T Z_C}, \\ &F_{44} = \tfrac{1}{R^2}, && F_{55} = \tfrac{1}{S^2}, && F_{66} = \tfrac{1}{T^2}, \\ &F_{12} = -\tfrac{1}{2}\tfrac{1}{\sqrt{X_T X_C Y_T Y_C}}, && F_{13} = -\tfrac{1}{2}\tfrac{1}{\sqrt{X_T X_C Z_T Z_C}}, && F_{23} = -\tfrac{1}{2}\tfrac{1}{\sqrt{Y_T Y_C Z_T Z_C}} \end{aligned} \tag{35}$$

where subscript T denotes tensile strengths, C denotes compressive strengths. X, Y and Z are the strengths in L, T and T' directions, respectively. R, S and T are shear strengths in TT', LT' and LT planes, respectively. T' is perpendicular to plane LT (see Fig. 1).

6. Results and discussion

The shape optimization process requires computation of constraint information (here, first-ply failure criterion). In order to guarantee the reliability of the constraint information, the accuracy of the plate model (and its implementation), the discretization procedure and postprocessing module have to be established. In this section, a detailed validation study for the plate model, along with the influence of mesh refinement and p-enrichment, is done. Further, a validation study for first-ply failure load is also carried out. This is followed by the shape optimization problem with and without adaptivity. The mesh types or patterns used in the study for plate model validation are shown in Fig. 5.

6.1. Comparison of displacement and stress components

In this section, first we define the problem for validation study. It is followed by validation studies for thick, moderately thick and thin laminates. Lastly, the validation study for first-ply failure load of laminates is presented.

Remark: The definition of thin, moderately thick and thick plates depends upon length to thickness ratio ($S = \frac{X}{d}$), loadings, boundary conditions, etc. In general, this definition is based on thickness ratio. Hence, we have used this definition in this analysis. Further, unless specified, the analysis is done for full laminate.

A laminated plate of dimensions X and Y along x and y directions, respectively, and thickness d, as shown in Fig. 1, has been considered for the analyses. The coordinate system and laminate sequence convention are also shown in this figure. The plate is

Table 1
Comparison of non-dimensionalized transverse deflection for square cross-ply thick plate under sinusoidal loading with mesh refinement and $p = 3$ fixed.

Mesh pattern	$\bar{w}_0$	$\Pi_p\left(\times 10^{-5}\right)$
Mesh-I	−1.9230	−1.7371
Mesh-II	−1.9242	−1.7395
Mesh-III	−1.9258	−1.7397
Mesh-IV	−1.9260	−1.7397
Kant et al. [38]	−1.9058	–

Table 2
Comparison of non-dimensionalized transverse deflection for square cross-ply thick plate under sinusoidal loading with p refinement for Mesh-III.

p	$\bar{w}_0$	$\Pi_p\left(\times 10^{-5}\right)$
1	−1.8339	−1.6009
2	−1.9267	−1.7388
3	−1.9258	−1.7397
4	−1.9261	−1.7397
Kant et al. [38]	−1.9058	–

Table 3
Material properties used for rectangular $[0/90]_S$ thick laminate under transverse sinusoidal loading [35].

Property	E_1 GPa	E_2 GPa	$G_{12} = G_{13}$ GPa	G_{23} GPa	$\nu_{12} = \nu_{13}$	ν_{23}
Value	138	9.3	4.6	3.1	0.3	0.5

Table 4
Comparison of transverse deflection for rectangular cross-ply thick plate under sinusoidal loading with mesh refinement for fixed $p = 3$.

Mesh pattern	$w_0\left(\times 10^{-4}\right)$	$\Pi_p\left(\times 10^{-4}\right)$
Mesh-I	−5.8090	−3.1683
Mesh-II	−5.8439	−3.1954
Mesh-III	−5.8467	−3.1974
Mesh-IV	−5.8468	−3.1975
3D solid [35]	−5.7263	−3.0851

Table 5
Comparison of transverse deflection for rectangular cross-ply thick plate under sinusoidal loading with p refinement for fixed Mesh-III.

p	$w_0\left(\times 10^{-4}\right)$	$\Pi_p\left(\times 10^{-4}\right)$
1	−5.2480	−2.8603
2	−5.8439	−3.1954
3	−5.8467	−3.1975
4	−5.8469	−3.1975
3D solid [35]	−5.7263	−3.0851

loaded transversely on the upper surface through a sinusoidal load as

$$q_z(x,y) = -q_c \sin\left(\frac{m\pi x}{X}\right) \sin\left(\frac{n\pi y}{Y}\right) \tag{36}$$

or with uniformly distributed transverse load as

$$q_z(x,y) = -q_0 \tag{37}$$

where q_c is the amplitude of the sinusoidal loading and q_0 is the intensity or magnitude of the uniform transverse load. The transverse mid-plane displacement at the center of the plate (that is, at $z = 0$), w_0 (unless specified) is normalized as $\bar{w}_0$

$$\bar{w}_0 = w_0 \frac{E_2 d^3}{q_c X^4} 10^2 \tag{38}$$

In above equation, when the load is uniformly distributed, the term q_c is replaced by q_0. Unless specified, in all problems the mesh types used are shown in Fig. 5.

6.1.1. Comparison for thick laminates

In this section cross-ply square and rectangular laminates under transverse loads are studied for their predictive capabilities of pointwise transverse deflection and stress components. This study is carried out for different types of mesh patterns (as shown in Fig. 5) and degree of approximation ($p = 1$ and 2) used. The results are compared with those available in literature.

Case 1: A cross-ply square laminate under sinusoidal transverse loading

A $[0/90/0]$ square laminated plate and $S = 5$, under sinusoidal transverse load, with $q_c = 6.89 \times 10^{-3}$ N/mm^2 and $m = n = 1$, is analyzed. The plate is simply supported over all edges. The lamina has properties $E_2 = E_3 = 6.89$ GPa and $\nu_{12} = \nu_{23} = \nu_{13} = 0.25$. Further, $E_1 = 25\,E_2, G_{23} = 0.2\,E_2$ and $G_{13} = G_{12} = 0.5\,E_2$ is taken. Here, all the laminae have equal thicknesses.

The comparison of non-dimensionalized transverse deflection with mesh refinement when $p = 3$ is fixed, is reported in Table 1. Table 2 reports these results for p refinement with mesh fixed to Mesh-III.

From these tables we can see that the values of non-dimensionalized transverse deflection from our study are close to the one with reference results obtained by Kant et al. [38]. For approximation order $p = 3$ the effect of mesh refinement shows that results converge with mesh refinement above Mesh-III and with p refinement it converges for $p \geqslant 3$. It should be noted that the reference results are obtained for a fixed rectangular mesh with four elements and no convergence analysis has been reported. Hence, we see a difference in the two results. Further, it can be seen that the total potential converges to a value of -1.7397×10^{-5} and for this value of total potential we observe that the non-dimensionalized transverse deflection also shows convergence.

Case 2: A cross-ply rectangular laminate under sinusoidal transverse loading

A rectangular $[0/90]_S$ laminated plate, hard simple supported along all edges, and subjected to transverse sinusoidal loading is analyzed. All the layers have equal thicknesses and $S = 5$ is taken. The laminae properties are listed in Table 3. The amplitude of sinusoidal loading q_c is 1 N/mm^2 with $m = n = 1$. The sinusoidal loading in this case is of the from

$$q_z(x,y) = -q_c \cos\left(\frac{m\pi x}{X}\right) \cos\left(\frac{n\pi y}{Y}\right) \tag{39}$$

Table 6
Comparison of stresses for rectangular cross-ply thick plate under sinusoidal loading with mesh refinement for fixed $p = 3$.

Mesh pattern	$\sigma^*_{xx}\left(\frac{X}{2},\frac{Y}{2},-\frac{d}{2}\right)$	$\sigma^*_{yy}\left(\frac{X}{2},\frac{Y}{2},-\frac{d}{2}\right)$	$\tau^*_{xy}\left(X,Y,-\frac{d}{2}\right)$	$\sigma_{xx}\left(\frac{X}{2},\frac{Y}{2},-\frac{d}{2}\right)$	$\sigma_{yy}\left(\frac{X}{2},\frac{Y}{2},-\frac{d}{2}\right)$	$\tau_{xy}\left(X,Y,-\frac{d}{2}\right)$
Mesh-I	8.5821	1.8848	−0.9662	8.0526	1.7647	−0.8916
Mesh-II	7.9947	1.7597	−0.9057	7.9523	1.7496	−0.8990
Mesh-III	7.9137	1.7410	−0.8989	7.9118	1.7403	−0.8982
Mesh-IV	7.9042	1.7384	−0.8980	7.9042	1.7382	−0.8970
3D solid [35]	7.7388	1.9267	−0.8602	7.7388	1.9267	−0.8602

Table 7
Comparison of stresses for rectangular cross-ply thick plate under sinusoidal loading with p refinement for fixed Mesh-III.

p	σ^*_{xx} $\left(\frac{X}{2},\frac{Y}{2},-\frac{d}{2}\right)$	σ^*_{yy} $\left(\frac{X}{2},\frac{Y}{2},-\frac{d}{2}\right)$	τ^*_{xy} $\left(X,Y,-\frac{d}{2}\right)$	σ_{xx} $\left(\frac{X}{2},\frac{Y}{2},-\frac{d}{2}\right)$	σ_{yy} $\left(\frac{X}{2},\frac{Y}{2},-\frac{d}{2}\right)$	τ_{xy} $\left(X,Y,-\frac{d}{2}\right)$
1	7.1042	1.5524	−0.8073	6.9450	1.5100	−0.7813
2	7.9947	1.7597	−0.9057	7.9523	1.7496	−0.8990
3	7.8687	1.7298	−0.8936	7.8972	1.7363	−0.8970
4	7.8663	1.7513	−0.8980	7.8980	1.7365	−0.8972
3D solid [35]	7.7388	1.9267	−0.8602	7.7388	1.9267	−0.8602

Table 8
Comparison of non-dimensionalized transverse deflection for a square cross-ply, moderately thick plate with mesh refinement and $p = 3$ fixed.

Mesh pattern	$\bar{w}_0$	$\Pi_p\left(\times 10^{-4}\right)$
Mesh-I	−0.7174	−1.0098
Mesh-II	−0.7171	−1.0127
Mesh-III	−0.7176	−1.0129
Mesh-IV	−0.7176	−1.0129
Kant et al. [38]	−0.7164	–

The transverse deflection for mesh refinement with fixed $p = 3$ is tabulated in Table 4 and for p refinement with Mesh-III is reported in Table 5. The convergence of the in-plane stress components has been reported in Table 6 for mesh refinement with $p = 3$ fixed and in Table 7 for p refinement with Mesh-III fixed. In Tables 6 and 7, the stress components $\sigma^*_{xx}, \sigma^*_{yy}$ and τ^*_{xy} denote recovered stresses and σ_{xx}, σ_{yy} and τ_{xy} denote finite element stresses. The recovered stresses are obtained using constitutive relations and the recovered strain components, as discussed in Section 3.1. These results are compared with the 3D finite element results reported in [35]. It should be noted that the origin of the coordinate system for laminate geometry in the present study is fixed at the lower left corner and in [35] it is fixed at the center of the laminate. From the results we observe that:

1. The results for transverse deflection converge to -5.8467×10^{-4} for mesh refinement with meshes above Mesh-III type and $p = 3$ fixed. The results from present study are close to 3D finite element results reported in [35].
2. The results from present study for deflection component with p refinement converge with Mesh-III fixed for $p \geqslant 3$. The converged values are same as mentioned in point 1 above.
3. The plate model gives a converged total potential value of -3.1975×10^{-4}, which is higher than the reference values in [35]. This difference between total potential values is because the plate model considered here assumes a smooth strain field through the thickness, which may lead to a jump in the values of the transverse stresses at the interfaces. This is in direct violation of the stress continuity requirement (from 3D elasticity solution point of view) at the interface.
4. The convergence of stress components to the values reported in [35], obtained using three dimensional finite element analysis, does not show much difference between stress components obtained using recovery and finite element approach for mesh refinement with $p = 3$. However, for p refinement, with mesh fixed, the recovered stress components show faster convergence to the values in [35] than compared to the convergence of finite element stress components.

Table 9
Comparison of non-dimensionlaized transverse deflection for a square cross-ply, moderately thick plate with p refinement and Mesh-III fixed.

p	$\bar{w}_0$	$\Pi_p \times 10^{-4}$
1	−0.6202	−0.8459
2	−0.7175	−1.0118
3	−0.7176	−1.0129
4	−0.7176	−1.0129
Kant et al. [38]	−0.7164	–

6.1.2. Comparison for moderately thick laminates

In this section square cross-ply anti-symmetric laminates under uniformly distributed transverse load are studied for their predictive capabilities of pointwise transverse deflection. This study is carried out for different types of mesh patterns (as shown in Fig. 5) and degree of approximation ($p = 1$ through 4) used. Then these results are compared with the results available in literature.

Case 1: A cross-ply square laminate under sinusoidal transverse loading

The problem description is same as Case 1 of the Section 6.1.1, but with $S = 10$. The effect of mesh refinement, with approximation order $p = 3$, on the convergence of the results has been studied and is reported in Table 8. Similarly, with Mesh-III fixed the effect of p refinement on the convergence of the results is reported in Table 9. Further, for these cases the convergence of the total potential is also reported.

The observations for this study show that the non-dimensionalized transverse displacement convergences to a value of -0.7176 and total potential to a value of -1.0129×10^{-4} for Mesh-III and higher levels of mesh refinement. Similarly, for Mesh-III the convergence is observed for $p \geqslant 3$. It can be observed that the convergence in the non-dimensionalized transverse displacement is seen when the value for total potential is converged. It can be easily seen that the converged value of the non-dimensionalized transverse displacement is very close to the value reported in [38]. Further, it can be observed that the convergence with mesh and p refinements is achieved faster as compared to thick plate case.

Case 2: An anti-symmetric square laminate under uniform transverse loading

A four-layer antisymmetric angle-ply square laminate, $[45/-45/45/-45]$, subjected to uniformly distributed transverse load is analyzed for all edges hard simple supported and all edges clamped boundary conditions. The intensity of the uniformly distributed load is $q_0 = 6.89 \times 10^{-3}$ N/mm^2. Here, the thicknesses of

Table 10
Comparison of non-dimensionalized transverse displacement for $[45/-45/45/-45]$ square, moderately thick laminate with mesh refinement for $p = 3$ fixed.

Boundary condition	Mesh pattern	$\bar{w}_0$	$\Pi_p\left(\times 10^{-4}\right)$
H-SSSS	Mesh-I	−1.1062	−2.6566
	Mesh-II	−1.1059	−2.6682
	Mesh-III	−1.1068	−2.6698
	Mesh-IV	−1.1069	−2.6700
	Reddy and Miravete [56]	−1.1598	–
CCCC	Mesh-I	−0.5562	−1.1342
	Mesh-II	−0.5779	−1.1756
	Mesh-III	−0.5799	−1.1819
	Mesh-IV	−0.5800	−1.1812
	Reddy and Miravete [56]	−0.7708	–

Table 11
Comparison of non-dimensionalized transverse displacement for $[45/-45/45/-45]$ square, moderately thick laminate with p refinement for fixed Mesh-III.

Boundary condition	p	$\bar{w}_0$	$\Pi_p \times 10^{-4}$
H-SSSS	1	−0.8862	−2.0615
	2	−1.1055	−2.6642
	3	−1.1068	−2.6698
	4	−1.1069	−2.6700
	Reddy and Miravete [56]	−1.1598	–
CCCC	1	−0.4632	−0.9143
	2	−0.5773	−1.1719
	3	−0.5799	−1.1819
	4	−0.5801	−1.1812
	Reddy and Miravete [56]	−0.7708	–

all layers are same and $S = 4$ is taken. The properties of the laminate material are: $E_2 = 6.89 \times 10^3$ N/mm^2, $\nu_{12} = \nu_{13} = 0.25, E_1 = 10E_2, G_{12} = G_{13} = 0.6E_2$, and $G_{23} = 0.5E_2$.

The convergence study for the values of non-dimensionalized transverse deflection and total potential has been carried out for both mesh and p refinements. These results are tabulated in Table 10 and Table 11, respectively. Here, H-SSSS or CCCC denote the boundary conditions that all edges are hard simple supported or clamped, respectively.

The observations drawn from this study are:

1. Both non-dimensionalized transverse displacement and total potential converge for mesh refinements above Mesh-III, whereas, for a fixed mesh Mesh III, the convergence with p refinement can be seen for $p \geqslant 3$. Further, the convergence for displacement component is seen when there is convergence for total potential as well.
2. The displacements from present study are higher than those obtained by Reddy and Miravete [56]. We have used higher order shear deformation theory (HSDT) while in [56] first order shear deformation plate theory (FSDT) is used. The solution to the problem is obtained by using Lévy method with state-space approach. The HSDT model leads to a more flexible structure as compared to the FSDT model. However, one should note that there is no significant difference in the values obtained by these models for hard simple supported boundary condition case. However, for all edges clamped boundary condition the results from present study are not in good agreement with [56]. This is due to the locking effect caused by edge constraints.
3. In both the studies, the results converge fast for simple supported plate as compared to the clamped one. The clamped plate shows significant effect of edge constraints, in comparison to the simple supported plate.

6.1.3. Comparison for thin laminates

In this section the non-dimensionalized transverse deflection is validated for cross-ply square laminate under sinusoidal load and cross-ply rectangular laminate under uniform transverse load for both mesh and p refinements.

Case 1: A cross-ply square laminate under sinusoidal transverse loading

The problem description is same as in Case 1 in Section 6.1.1 with the change that $S = 100$. The results from present study are given in Table 12 and Table 13. From above tables we can see that:

1. The non-dimensionalised displacement converges to −0.4353 and total potential to −0.0614 for mesh refinement Mesh-III and $p = 3$ fixed and similar results are seen for fixed mesh Mesh-III and p refinement with $p \geqslant 3$.
2. The non-dimensional displacement obtained from present study is very close to the reference values in [38]. It should be noted that the laminate considered here is thin. Hence, the effect in transverse direction is easily captured by HSDT model used in the present study.
3. The convergence in both displacement and total potential values is achieved with a moderate mesh and p refinements.

Case 2: A cross-ply rectangular laminate under uniform transverse loading

A simply supported thin cross-ply laminate $[0/90]_S$ with thickness of each ply as 0.127 mm and $S \approx 450$ under uniformly distributed load is considered. The intensity of the uniform load applied is $q_0 = 6.9 \times 10^{-4}$ MPa. T300/5208 Graphite/Epoxy (pre-preg) $(v_f = 0.7)$ is used as the material for the laminate analyzed. The material properties for this material are given in Table 14. Results are tabulated in Table 15 and Table 16. From these tables, it can be observed that:

1. The displacement converges to a value of −11.5004 with mesh refinement for mesh refinement level of Mesh-III or above.
2. The convergence with refinement for the Mesh-III or above levels is achieved with $p \geqslant 3$.
3. The reference results are obtained for constant mesh and with FSDT model. Also, no convergence study with respect to either mesh refinement or p refinement was done. The results with present HSDT model match exactly with the results reported in [56].
4. Mesh refinement level Mesh-III and $p = 3$ seem to be reasonable for convergence study.

6.2. First-ply failure load

In this section, the first-ply failure load using Tsai-Wu failure theory [33] has been obtained. The transverse deflection at the center of the plate corresponding to the first-ply failure load is also obtained. These results are then compared with the results reported in [57].

The non-dimensionalized transverse deflection at the center of the plate, corresponding to the first-ply failure load, is defined as

$$w_0^* = \frac{w_0}{d} \tag{40}$$

and the non-dimensionalized first-ply failure load (*FLD*) is given by

Table 12
Comparison of non-dimensionalized transverse displacement for thin cross-ply laminate with mesh refinement for $p = 3$ fixed.

Mesh pattern	$\bar{w}_0$	Π_p
Mesh-I	−0.4336	−0.0605
Mesh-II	−0.4352	−0.0612
Mesh-III	−0.4353	−0.0614
Mesh-IV	−0.4353	−0.0614
Kant et al. [38]	−0.4344	–

Table 13
Comparison of non-dimensionalized transverse displacement for thin cross-ply laminate with p refinement for fixed Mesh-III.

p	$\bar{w}_0$	Π_p
1	−0.0388	−0.0530
2	−0.4255	−0.0600
3	−0.4353	−0.0614
4	−0.4353	−0.0614
Kant et al. [38]	−0.4344	–

Table 14
Material properties for T300/5208 Graphite/Epoxy unidirectional composite [56].

Property	E_1 GPa	$E_2 = E_3$ GPa	$G_{12} = G_{13}$ GPa	G_{23} GPa	$\nu_{12} = \nu_{13}$	ν_{23}
Value	132.5	10.8	5.7	3.4	0.24	0.49

Table 15
Comparison of non-dimensionalized transverse displacement for cross-ply thin laminate with mesh refinement and fixed $p = 3$.

Mesh pattern	w_0^*	Π_p
Mesh-I	−11.7421	−23.9584
Mesh-II	−11.5132	−24.2721
Mesh-III	−11.5004	−24.4141
Mesh-IV	−11.5004	−24.4231
Reddy et al. [56]	−11.5000	–

Table 16
Comparison of non-dimensionalized transverse displacement for cross-ply thin laminate with p refinement for fixed Mesh-III.

p	w_0^*	Π_p
1	−0.0340	−0.0712
2	−10.9555	−23.2155
3	−11.5004	−24.4141
4	−11.5004	−24.4250
Reddy et al. [56]	−11.5000	–

$$FLD = \frac{q_0}{E_2}\left(\frac{X}{d}\right)^4 \tag{41}$$

For this validation study, the mesh topology shown in Fig. 5 has been used. First, an antisymmetric angle ply laminated plate is studied for its first-ply failure load. In the second problem, we have analyzed a symmetric cross ply laminate for its first-ply failure load. The first-ply failure load has been obtained by using finite element stresses as well as stresses constructed using recovered strains and constitutive relations. In both cases the transverse stresses used are obtained by using equilibrium equations.

Case 1: Antisymmetric angle-ply laminate under uniformly distributed load

The problem description is same as Case 2 in Section 6.1.3. The antisymmetric angle ply laminated plate considered here is clamped along all edges and loaded with uniformly distributed transverse load. This laminate with material T300/5208 Graphite/Epoxy (pre-preg) is analyzed for first-ply failure load. The material strength parameters are given in Table 17.

Table 17
Strength parameters for T300/5208 Graphite/Epoxy unidirectional composite [57].

Property	X_T	X_C MPa	$Y_T = Z_T$ MPa	$Y_C = Z_C$ MPa	R MPa	$S = T$ MPa
Value	1515	1697	43.8	43.8	67.6	86.9

Results from our analysis are reported in Table 18 for h refinement and in Table 19 for p refinement. In these tables RR denotes that the stresses constructed from recovered strains are used in failure criterion in Eq. (34) and FE denotes finite element stresses along with Eq. (41). Here and in the following, 'xco' and 'yco' denote the x and y coordinates of the point where the failure index value is reported.

From the above tables we can see that:

1. For fixed value of $p = 2$ with mesh refinement, the failure load for Mesh-II is very high. This is due to locking effect exhibited by plate. Since, plate is very thin and clamped along all edges, this effect is more severe. A similar observation can be made for p refinement.
2. With higher levels of refinement for mesh (Mesh-IV) or higher p values the failure loads are very close to one reported in [57].
3. The failure loads with stresses obtained from recovered strains are lower compared to failure load obtained by using finite element stresses.
4. The failure locations obtained for our study are different from those reported in [57]. The problem considered is symmetric in all respect. Hence, locations can also be expected to be symmetric. We are getting the locations on the face opposite to that obtained from reference results. It should be noted that the reference results were obtained for a fixed mesh with FSDT model using Lagrangian iso-parametric rectangular elements and no convergence study was done.
5. Failure location is found mostly on top face of the laminate. Further, the maximum contribution to failure index is due to σ_{xx} and τ_{xy} stress components. The failure mode is, thus, matrix failure.

Case 2: A cross-ply laminate under uniformly distributed load

The problem description is same as in Case 1 above, but the lamination scheme for this problem is $[0/90]_S$. Results from present analysis are reported in Table 20 for mesh refinement with $p = 2$ held constant and in Table 21 with p refinement for a constant mesh, Mesh-II.

The comparison of the results with the reference results yield the same conclusions as discussed in Case 1 above.

Fig. 6 depicts the failure locations obtained from present study and those reported in [57]. The point 1^* and 2^* denote the failure locations obtained by Reddy and Reddy [57] for $[-45/45/-45/45]$ and $[0/90]_S$ laminates, respectively. Further, the points $1^\bullet$ and $2^\bullet$ show the failure locations from our study for $[-45/45/-45/45]$ and $[0/90]_S$ laminates, respectively. A detailed study on the first-ply failure loads along with discretization error control can be seen in earlier works of authors [49].

Table 18
Comparison study for first-ply failure load for $[-45/45/-45/45]$ laminate with h refinement for $p = 2$ fixed.

Mesh pattern	Stress type	FLD	w_0^*	xco	yco	Ply number	Location
Mesh-II	RR	1.771×10^6	−35.09	111.93	2.84	1	Top
	FE	1.223×10^6	−24.25	166.62	93.82	4	Bottom
Mesh-III	RR	46264.58	−25.77	115.78	1.42	1	Top
	FE	55555.74	−30.94	111.93	0.71	1	Top
Mesh-IV	RR	37661.66	−23.85	115.35	0.95	1	Top
	FE	41294.01	−26.15	112.79	0.47	1	Top
Reddy et al. [56]	FE	39354.80	−26.79	≈ 125	≈ 125	1	Top

Table 19
Comparison study for first-ply failure load for $[-45/45/-45/45]$ laminate with p refinement for fixed Mesh-II.

p	Stress type	FLD	w_0^*	xco	yco	Ply number	Location
2	RR	1.771×10^6	−35.09	111.93	2.34	1	Top
	FE	1.223×10^6	−24.25	166.62	93.82	4	Bottom
3	RR	38044.02	−25.66	129.31	125.83	1	Top
	FE	35558.73	−24.10	119.62	125.57	1	Top
4	RR	32385.21	−21.92	99.68	125.83	1	Top
	FE	29058.74	−19.64	176.87	3.32	1	Top
Reddy et al. [56]	FE	39354.80	−23.79	≈ 125	≈ 125	1	Top

Table 20
Comparison study for first-ply failure load for $[0/90]_S$ laminate with h refinement for $p = 2$ fixed.

Mesh type	Stress type	FLD	w_0^*	xco	yco	Ply number	Location
Mesh-II	RR	1.215×10^6	−24.38	117.06	2.84	4	Bottom
	FE	1.173×10^6	−23.53	119.62	1.42	1	Top
Mesh-III	RR	26955.81	−21.92	115.78	1.42	1	Top
	FE	29899.92	−24.32	117.06	0.71	1	Top
Mesh-IV	RR	19499.95	−18.41	115.35	126.05	1	Top
	FE	21029.35	−19.85	112.79	126.52	1	Top
Reddy et al. [56]	FE	19050.90	−19.34	≈ 2	≈ 75	1	Top

Table 21
Comparison study for first-ply failure load for $[0/90]_S$ laminate with p refinement for fixed Mesh-II.

p	Stress type	FLD	w_0^*	xco	yco	Ply number	Location
2	RR	1.215×10^6	−24.38	117.06	2.84	4	Bottom
	FE	1.738×10^6	−19.58	119.62	1.42	1	Top
3	RR	19423.48	−19.58	109.37	1.42	1	Top
	FE	17588.19	−17.80	119.62	125.57	1	Top
4	RR	16823.48	−16.97	119.62	1.42	1	Top
	FE	15676.43	−15.82	119.62	125.57	1	Top
Reddy et al. [56]	FE	19050.90	−19.34	≈ 2	≈ 75	1	Top

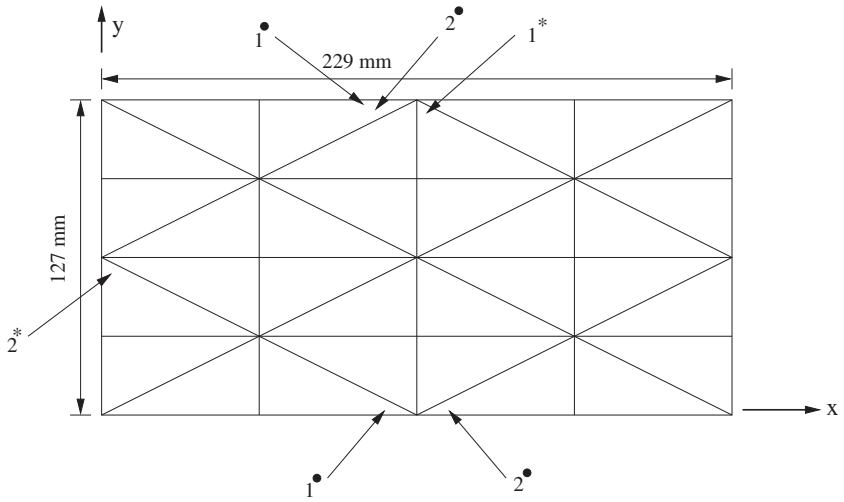

Fig. 6. Laminate showing the failure locations predicted from present study and reported in [57].

Remark: In above example cases the transverse normal stress, that is σ_{33}, is not considered while evaluating the failure index in Eq. (34). This is because this component cannot be computed either from recovered strain data or finite element data, directly. Further, no attempt has been made to evaluate this component using equilibrium equations.

6.3. Shape optimization

Here, with few typical examples, we will demonstrate the effect of control of discretization error on the final "optimal" shape of the cutout and value of failure index attained. In this study, cross-ply and angle-ply symmetric laminates with cutouts have been studied.

Remark: In each of the problems, we start with an initial profile of the elliptical cutout to be circular with $a = b = Y/8$, and $\theta = 0^\circ$. Since the $p = 2$ approximation, with sufficiently refined mesh, gives reasonable failure load values, this is taken as the order of approximation for all future computations.

6.3.1. A rectangular $[0/90]_S$ laminate under transverse uniform loading

A rectangular symmetric laminated plate, with a cutout, clamped along one of the smaller edge (that is, $x = 0$) and loaded transversely with uniformly distributed load, is analyzed for shape optimization. The intensity of the transverse uniform load is $q_0 = 2.0\ \mathrm{N/mm^2}$. The lamination scheme considered is $[0/90]_S$ with $S = 10$. Here, $Y = \frac{X}{2}$ is taken.

All laminae are made of T300/5208 Graphite/Epoxy (pre-preg) and have a thickness of 0.127 mm. The material mechanical properties are given in Table 14 and strength parameters are given in Table 17. Here, $p = 2$ is used in the study.

The optimum cutout shape results are tabulated in Table 22 and the corresponding cutout shapes during optimization process are shown in Fig. 7. From these results we observe that:

1. The discretization errors are below 5% for all the feasible shapes. Hence, adaptive refinement is not needed.
2. The initial configuration with the given loading had a maximum failure index of 0.4095. Thus, there was scope for reduction in weight by increasing the size of cutout, which in turn may increase the failure index value. This fact is seen through the intermediate configuration during the optimization procedure. The size of the cutout is increased, thereby increasing the maximum value of failure index.
3. The maximum failure index for optimal solution is very close to the allowable value set (FLD $\leqslant$ 0.8).
4. The reduction in weight for this study is 3.68%.

Table 22
Optimal shape for cutout in $[0/90]_S$ laminate without adaptive refinement and $p = 2$.

Sequence	a	b	Weight	Max. index	error (%)	xco	yco
Initial	0.3175	0.3175	12.5865	0.4095	3.6582	2.2109	1.2165
Intermediate	0.5799	0.4109	12.1544	0.7709	4.8672	1.9517	1.3472
Intermediate	0.6015	0.4119	12.1245	0.7899	4.3852	1.9197	1.2083
Optimal	0.6057	0.4100	12.1229	0.7959	4.8293	1.9157	1.2077

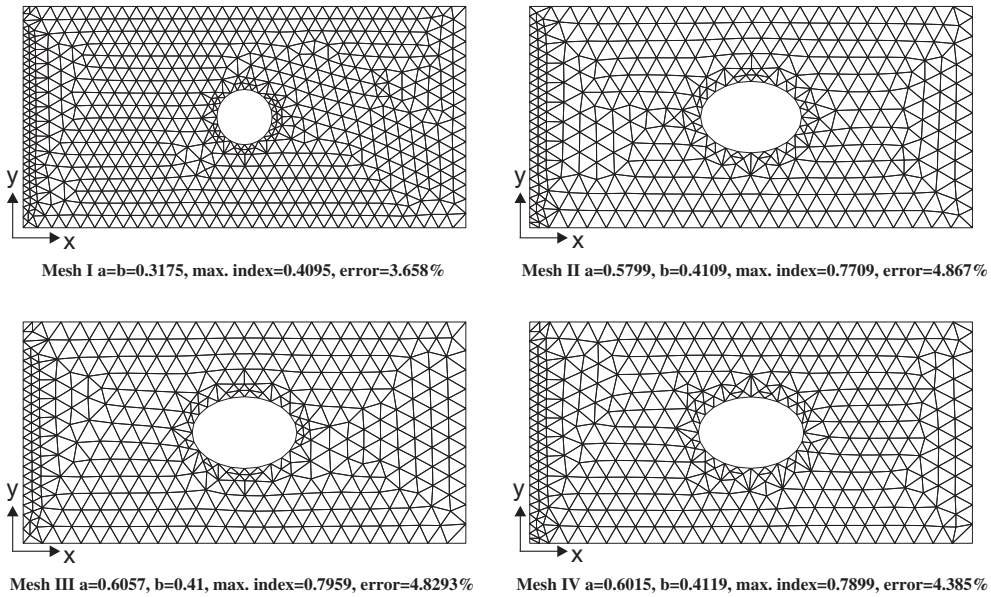

Fig. 7. Cutout shapes during optimization in $[0/90]_S$ laminate under uniform transverse load.

Table 23
Optimal shape for cutout in $[45/-45]_S$ laminate without adaptive refinement and $p = 2$.

Sequence	a	b	Weight	Max. index	error (%)	xco	yco
Initial	0.3175	0.3175	12.5865	0.4953	7.1979	0.0740	0.0224
Intermediate	0.8598	0.8808	10.5236	0.3461	11.8820	2.1983	0.4315
Intermediate	1.0122	0.8960	10.0535	0.3939	11.8937	2.1435	0.4188
Optimal	1.0160	1.0160	09.6602	0.7712	15.6503	2.4090	2.3167

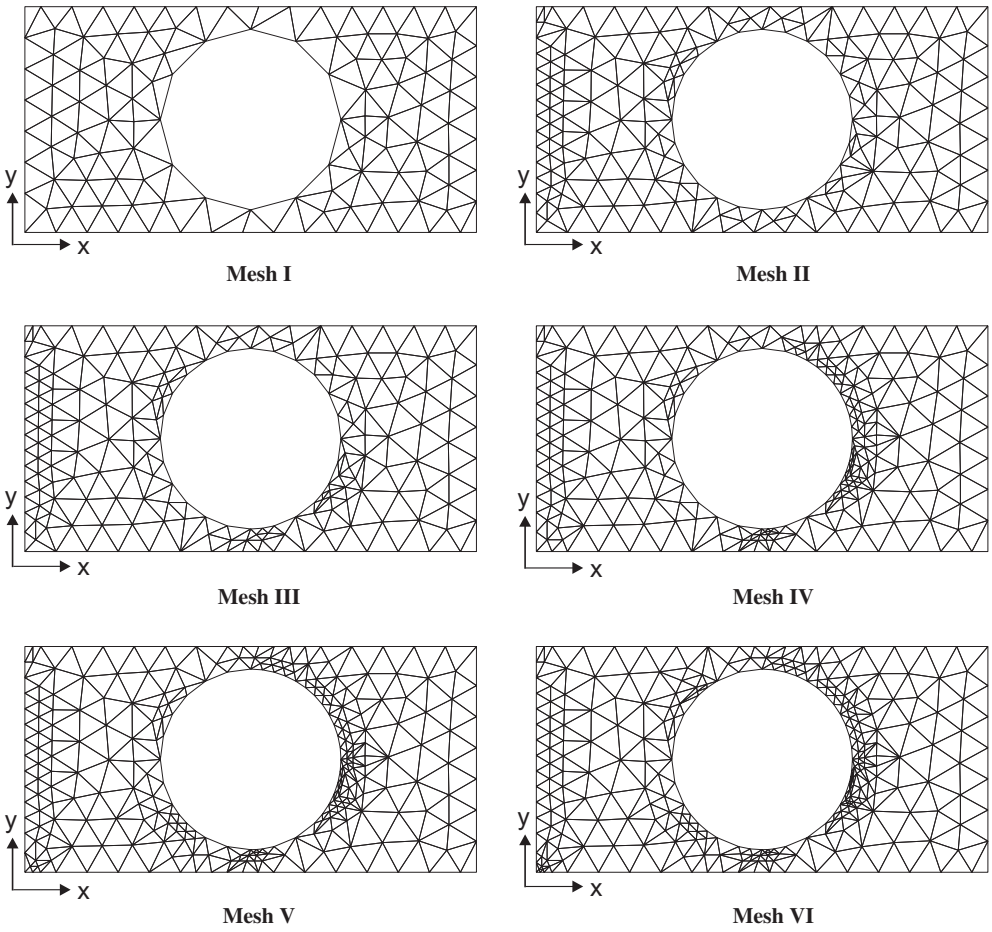

Fig. 8. Adaptive refinements in optimum shape for $[45/-45]_S$ laminate under uniform transverse load.

Table 24
Effect of adaptivity on final optimal shape in $[45/-45]_S$ laminate under transverse uniform load.

Refinement level	error (%)	Max. index
Initial	15.6503	0.7712
First	15.0825	–
Second	13.5012	–
Third	12.4125	–
Fourth	11.0823	–
Fifth	10.4591	1.0089

Table 25
Effect of adaptivity on optimal shape in $[45/-45]_S$ laminate subjected to uniform transverse loading.

Adaptivity	a	b	Weight	Max. index	error (%)
No	1.0160	1.0160	09.6602	0.7712	15.6503
Yes	0.5248	0.3175	12.3796	0.7978	6.7000

5. The failure occurs at the edges of cutout boundary. When the contribution to the failure index from each of the stress component is studied in detail, it was seen that the stress component σ_{yy} contributes more as compared to other components. Thus, the mode of failure can be said to be a matrix failure. This result is in accordance with the results obtained by Ericson et al. [58].
6. The optimal shape of the cutout is an ellipse with an orientation angle of 0° with respect to x axis.

Table 26
Effect of adaptivity on optimal shape in $[45/-45]_S$ laminate subjected to combined loading.

Adaptivity	a	b	Weight	Max. index	error (%)
No	1.0155	0.8753	10.1103	0.7997	8.3792
Yes	1.0157	0.8258	10.2681	0.7999	6.4297

6.3.2. A rectangular $[45/-45]_S$ laminate under transverse uniform loading

The problem description is same as in Section 6.3.1. However, in this case the lamination scheme is changed to $[45/-45]_S$. The intensity of uniform transverse load is $q_0 = 0.22$ N/mm^2.

In this study the discretization error was estimated but not controlled by adaptive refinements. These results are tabulated in Table 23. From these results we observe that:

1. The discretization errors are above 10% in most of the feasible shapes.
2. The reduction in weight obtained is about 22%.
3. The final optimum shape has reached the upper bound on the design variables, that is, the minor and major axes of the elliptical cutout. Although, the value of failure index is very close to the allowable value set for this optimum shape, there is scope of additional material removal from this design.

4. Failure occurs at the edges of cutout boundary. This is due to high stress concentration because of constraint and free-edge effects. Further, it was observed that the location of first-ply failure changes from one iteration to another in the cutout vicinity.
5. When the contribution to failure index from each of the stress component at the point of failure was analyzed, it was seen that the stress components σ_{yy} and τ_{xy} contribute most. Thus, it can be said that the mode of failure in this case is matrix failure. This result is in accordance with experimental study reported by Herakovich [54].

In the above study the discretization error was not controlled. The discretization error for the optimal shape is over 15%. Now, without changing the optimal shape obtained, an attempt is made to control the discretization error below 7% or five refinement levels, whicever is attained earlier. The sequence of adaptive mesh refinements is shown in Fig. 8. Mesh-I is the initial mesh used. The discretization errors for these refined meshes are reported in Table 24.

The error estimator predicts that the elements of the clamped edge and the cutout boundaries have high discretization error. Hence, a relatively refined mesh is seen at these locations. This result is in agreement with the earlier study of the authors [46]. The higher discretization error near the constraint and free edges of the cutout are expected due to constraint and free-edge effects.

Thus, due to adaptive refinement the errors are reduced from 15.6503% to 10.4591%. However, the failure index has increased from 0.7712 to 1.0089. This shows that the optimal solution obtained without control over discretization error is unsafe. Hence, control of discretization error is essential in shape optimization study.

Now we will see the effect of discretization error control, through adaptive mesh refinements, on the outcome of the optimization process. The mesh is refined adaptively till either the tolerance in discretization error is reduced below 7% or for five levels of refinement, whichever is attained earlier. The comparison of results with and without adaptivity is shown in Table 25.

From these results it is seen that:

1. The final optimal shape obtained with and without adaptivity are significantly different. The optimal shape of the cutout without discretization error control is circular in nature while the one obtained with discretization error controlled throughout the optimization procedure is elliptic in shape with orientation of 0° with x-axis.
2. The discretization error for the final optimal shape with adaptive procedure is well below the tolerance mentioned.
3. Failure occurs at the cutout boundary, but the location changes from one iteration to another.
4. The value of the maximum failure index attained is very close to the allowable value.
5. The weight reduction in the optimal design obtained without control of discretization error (about 22%) is more compared to one obtained with control of discretization error (about 2%). Thus, from this example it is seen that if the discretization error is not controlled, more material removal will be predicted erronouysly, hence compromising safety of design.

6.3.3. A rectangular $[45/-45]_S$ laminate under combined loading

A rectangular symmetrically laminated composite plate, $[45/-45]_S$ clamped along a smaller edge, $x = 0$ is taken. The plate is loaded under uniformly distributed load, in-plane tensile loading and shear load. The laminate properties are as in Section 6.3.1. For this case, $q_0 = 0.15\ \text{N/mm}^2$, $N_{xx} = 20\ \text{N/mm}$ and $N_{xy} = 0.35\ \text{N/mm}$ are taken. Here, N_{xx} and N_{xy} denote uniform axial stress along x direction and shear stress in $x-y$ plane per unit length, respectively, applied on the edges.

In this study first the optimal cutout shape is obtained without controlling the discretization error and then the optimal shape is obtained with control of discretization error. Again, the mesh is refined adaptively till either the tolerance in discretization error is reduced below 7% or for five levels of refinement, whichever is attained earlier. The results are reported in Table 26. Here, we see that the final optimal shapes obtained with and without adaptivity are closer to each other in all respects. This is because the discretization error in both the cases is close. Further, it is seen that failure occurs near the cutout boundary, but the location changes during the iterations. Thus, it can be concluded that if the discretization error is within specified tolerance, then there is no effect of adaptivity on final design. Note that using higher p ($p \geqslant 3$) will not result in significant change in the conclusions, as the discretization error is controlled.

Remark: The optimization algorithm used here works with a set of feasible points. In the present study the initial set of feasible shapes are chosen such that the failure index is closer to 0.8. Further, it is seen that during each iteration the feasible shape attained is such that failure index reaches close to the maximum value of 0.8. Therefore, the evolution of failure index with iterations will be almost a horizontal line. Further, it is interesting to see the evolution of optimal shape with iterations. Here, this has been depicted for Examples 6.3.1 and 6.3.2 for some of the iterations.

Remark: The proposed approach is very efficient as it simultaneously estimates and controls the discretization error in each iteration. The cost of computation involved with this approach, with lower value of approximation, can be significantly lower than that without the control of discretization error but a highly refined mesh and/or higher value of approximation. It was shown in [42,45] that recovered strain field is accurate than that obtained by the finite element solution. This leads to the accurate computations of stresses used in the optimization constraints evaluation. Further, it was shown in [42,45–47] that the ZZ type approach of estimating and controlling the discretization error is computationally economical. Therefore, the overall approach used for shape optimization is computationally economical and accurate as well.

Remark: Here, all computations have been carried out approximation order $p = 2$. This has been done intentionally because in all practical purpose computations a lower order of approximation is used. When a lower approximation order is used and discretization error is not controlled then final solution may not be accurate. Here, we wanted to demonstrate this fact through the optimization study. If the approximation order is increased then the recovered strains will be more accurate. Therefore, the discretization error will be lesser as compared to the error when obtained with $p = 2$. However, the final optimal shape obtained with higher approximation order may not be different from that one obtained with $p = 2$.

7. Conclusions

In this study the shape optimization of laminated composites plates with cutout has been studied with a special emphasis on control of the finite element discretization error. A third order shear deformation plate theory has been used for the laminate analysis and is implemented in a finite element code. A strain field having same representation as the exact solution of the displacement field of the plate model considered is recovered using energy projections over the element patches similar to ZZ type patch recovery. Then these recovered strains are used to define a-posteriori error estimator, which drives a simple mesh refinement

algorithm. The plate model used is tested for its accuracy in predicting transverse displacement component, stress components and first-ply failure load obtained using Tsai-Wu failure theory under various boundary; transverse loading conditions, plate thickness ratios and lamination schemes. An optimization algorithm using complex search method has been employed. Finally, the effect of discretization error control over the final optimal design is demonstrated through simple, yet effective examples. The key conclusions from this study can be given as follows:

1. For thick laminates, the plate model used needs moderately refined mesh and the cubic approximation order used is sufficient.
2. For moderately thick laminates, proper mesh refinement and approximation orders should be chosen for a better convergence.
3. For thin laminates, boundary layer effect is severe. Mesh refinements are needed in order to eliminate the effect of locking. Higher approximation orders ($p \geqslant 3$) is also needed in order to reduce the locking effect. Thus, for a thin plate greater care should be taken (with respect to the approximation) in order to ensure reliability of the solution quantities.
4. The transverse displacement component obtained for thick, moderately thick and thin cross-ply and angle ply laminates for various boundary conditions under uniform as well as sinusoidal transverse loads are accurate. Further, the stresses obtained using recovered strains are reasonably accurate.
5. For angle ply laminates the failure starts at the top or bottom edge of the laminate. The failure is dominated by σ_{yy} and τ_{xy} stress components. This results in matrix type failure in the laminate.
6. For cross-ply laminates, the failure starts at the top or bottom edge of the laminate. The failure mainly occurs due to stress component σ_{yy}. Again, this gives rise to matrix type failure in the laminate.
7. In case of laminates with cutout, the failure starts at the cutout boundary. This is because of high stresses due to free-edge effect at the cutout boundaries.
8. With the use of stresses obtained using recovered strains, failure is predicted earlier than that obtained using the finite element stresses. These failure loads are 5–18% lesser than the reported results for angle-ply laminates. Further, these values for failure load are about 12% lesser than the values reported in literature for cross-ply laminates.
9. Adaptive refinement procedure based on a-posteriori error estimation affects the final optimal solution. The final design obtained with a cruder approximation is dangerous, because more material removal is predicted if the discretisation error is high (20% more material removal predicted). This is because the plate behavior is stiffer with a crude approximation, as compared to that obtained with proper refinements and/or approximation order.
10. This study brings out the important point that it is imperative to have some indication of the discretisation error, in order to accept or reject the final design obtained from the shape optimization.

References

[1] Park WJ. An optimal design of simple symmetric laminates under the first ply failure criterion. J Compos Mater 1982;16:341–55.
[2] Fukunaga H, Sekine H. Optimum design of composite structures for shape, layer angle and layer thickness distributions. J Compos Mater 1993;27(15):1479–92.
[3] Abrate S. Optimal design of laminated plates and shells. Compos Struct 1994;29:269–86.
[4] Kam TY, Lai FM, Liao SC. Minimum weight design of laminated composite plates subject to strength constraint. AIAA J 1996;34(8):1699–708.
[5] Shin YS, Haftka RT, Watson LT, Plaut RH. Design of laminated plates for maximum buckling load. J Compos Mater 1989;23:348–69.
[6] Lee MS, Kikuchi N, Scott RA. Shape optimization laminated composite plates. Comput Methods Appl Mech Eng 1989;72:29–55.
[7] Adali S, Richter A, Verijenko VE, Summers EB. Optimal design of hybrid laminates with discrete ply angles for maximum buckling load and minimum cost. Compos Struct 1995;32:409–15.
[8] Adali S, Walker M, Verijenko VE. Multiobjective optimization of laminated plates for maximum prebuckling, buckling and postbuckling strength using continuous and discrete ply angles. Compos Struct 1996;35:117–30.
[9] Botkin ME. Shape optimization with buckling and stress constraints. AIAA J Technical Notes 1996;34(2):423–5.
[10] Nagendra S, Haftka RT, Gürdal Z. Design of a blade-stiffened composite panel with a hole. Compos Struct 1991;18:195–219.
[11] Naik NK, Ganesh VK. Optimum design studies on FRP beams with holes. Compos Struct 1993;24:59–66.
[12] Sivakumar K, Iyengar NGR, Deb K. Free vibration of laminated composite plates with cutout. J Sound Vib 1999;221(3):443–70.
[13] Haftka RT, Grandhi RV. Structural shape optimization – a survey. Comput Methods Appl Mech Eng 1986;57:91–106.
[14] Ding Y. Shape optimization of structures: a literature survey. Comput Struct 1986;24(6):985–1005.
[15] Sobieszczanski-Sobieski J, Haftka RT. Multidisciplinary aerospace design survey of recent developments. Struct Optim 1997;14:1–23.
[16] Kaufmann M, Zenkert D, Wennhage P. Integrated cost/weight optimization of aircraft structures. Struct Multidisc Optim 2010;41:325–34.
[17] Kikuchi N, Chung KY, Torigaki T, Taylor JE. Adaptive finite element methods for shape optimization of linearly elastic structures. Comput Methods Appl Mech Eng 1986;57:67–89.
[18] Hinton E, Özakca M, Rao NVR. An integrated approach to structural shape optimization of linearly elastic structures. Part II: Shape definition and adaptivity. Comp Sys Eng 1991;2:4156.
[19] Weck M, Nottebaum T. Adaptive meshing – saving computational costs during the optimization of composite structures. Struct Optim 1993;6:108–15.
[20] Bennett JA, Botkin ME. Structural shape optimization with geometric description and adaptive mesh refinement. AIAA J 1985;23(3):458–64.
[21] Schleupen A, Maute K, Ramm E. Adaptive FE-procedures in shape optimization. Struct Multidisc Optim 2000;19:282–302.
[22] Morin P, Nochetto RH, Pauletti MS, Verani M. Adaptive finite element method for shape optimization. ESAIM: Control Optim Calculus Variations 2012;18:1122–49.
[23] Tian X, Wang MY. h-Adaptive extended finite element method for structural optimization. 10th World Congress on Structural and Multidisciplinary Optimization. USA: Orlando, Florida; 2013.
[24] Bugeda G, Ródenas JJ, Oñate E. An integration of a low cost adaptive remeshing strategy in the solution of structural shape optimization problems using evolutionary methods. Comput Struct 2008;86:1563–78.
[25] Bruggi M, Veranio M. A fully adaptive topology optimization algorithm with goal-oriented error control. Comput Struct 2011;89:1481–93.
[26] Wang Y, Kang Z, He Q. An adaptive refinement approach for topology optimization based on separated density field description. Comput Struct 2013;117:10–122.
[27] Reddy JN. A simple higher-order theory for laminated plates. J Appl Mech 1984;51:74552.
[28] Zienkiewicz OC, Zhu JZ. A simple error estimator and the adaptive procedure for practical engineering analysis. Int J Numer Methods Eng 1987;24:337–57.
[29] Zienkiewicz OC, Zhu JZ. The superconvergent patch recovery and a-posteriori error estimates. Part 1: The recovery technique. Int J Numer Methods Eng 1992;33:1331–64.
[30] Rank E, Zienkiewicz OC. A simple error estimator in the finite element method. Comm Appl Numer Methods 1987;3:243–9.
[31] Zhu JZ, Zienkiewicz OC. Superconvergence recovery technique and a-posteriori error estimators. Int J Numer Methods Eng 1990;30:1321–39.
[32] Deb K. Optimization for Engineering Design, Algorithms and Examples. New Delhi: Prentice Hall of India Private Limited; 1998.
[33] Tsai SW, Wu EM. A general theory of strength for anisotropic materials. J Compos Mater 1971;5:58–80.
[34] Lo KH, Christensen RM, Wu EM. A higher-order theory of plate deformation – Part-2: Laminated plates. J Appl Mech 1977;44(4):616–69.
[35] Actis RL, Szabó BA, Schwab C. Hierarchic models for laminated plates and shells. Comput Methods Appl Mech Eng 1999;172(1–4):79–107.
[36] Pandya BN, Kant T. A refined higher-order generally orthotropic C0 plate bending element. Comput Struct 1988;28:119–33.
[37] Pandya BN, Kant T. Finite element stress analysis of laminated composite plates using a higher-order displacement model. Comp Sci Technol 1988;32:137–55.
[38] Pandya BN. Higher-order theories and finite element evaluations for multilayer composite plates. Ph.D. dissertation, Indian Institute of Technology Bombay, India; 1988.
[39] Babuška I, Strouboulis T. The finite element method and its reliability. Oxford: Oxford Science Publications; 2001.

[40] Verfürth R. A review of a-posteriori error estimation and adaptive mesh-refinement. New York: Wiley; 1996.
[41] Verfürth R. A review of a-posteriori error estimation techniques for elasticity problems. Comput Methods Appl Mech Eng 1999;176:419–40.
[42] Babuška I, Strouboulis T, Upadhyay CS, Gangaraj SK, Copps K. Validation of a-posteriori error estimators by numerical approach. Int J Numer Methods Eng 1994;37:1073–123.
[43] Babuška I, Strouboulis T, Mathur A, Upadhyay CS. Pollution error in the *h* version of the finite element method and the local quality of a-posteriori error estimators. Finite Elem Anal Des 1994;17:273–321.
[44] Babuška I, Strouboulis T, Upadhyay CS. A model study of the quality of a-posteriori error estimators for linear elliptic problems. Error estimation in the interior of patchwise uniform grids of triangles. Comput Methods Appl Mech Eng 1994;114:307–78.
[45] Upadhyay CS. Computer-based analysis of error estimation and superconvergence in finite element computations. Ph.D. dissertation at Texas *A&M* University, Texas; May 1997.
[46] Mohite PM, Upadhyay CS. A simple strain-recovery based a-posteriori error estimator for laminated composite plates. J Aerospace Sci Technol 2007;59(3):212–22.
[47] Mohite PM, Upadhyay CS. Local quality of smoothening based a-posteriori error estimators for laminated plates under transverse loading. Comput Struct 2002;80(18–19):1477–88.
[48] Mohite PM, Upadhyay CS. Focussed adaptivity for laminated plates. Comput Struct 2003;81(5):287–98.
[49] Mohite PM, Upadhyay CS. Accurate computation of critical local quantities in composite laminated plates under transverse loading. Comput Struct 2006;84(10–11):657–75.
[50] Mohite PM, Upadhyay CS. A generalized adaptive finite element analysis of laminated plates. Comput Struct 2012;112–113:217–34.
[51] Suri M, Babuška I, Schwab C. Locking effects in the finite element approximation of plate models. Math Comput 1995;64(210):461–82.
[52] Yunus SM, Pawlak TP, Wheeler MJ. Application of the Zienkiewicz-Zhu error estimator for plate and shell analysis. Int J Numer Methods Eng 1990;29:1281–98.
[53] Gastaldi L. Uniform interior error estimates for the Reissner–Mindlin plate model. Math Comp 1993;61(204):539–67.
[54] Herakovich CT. Mechanics of fibrous composites. Delhi: John Wiley and Sons, Inc; 1998.
[55] Mohite PM. Composite materials and structures, NPTEL course. http://nptel.ac.in/courses/101104010/.
[56] Reddy JN, Miravete A. Practical analysis of composite laminates. New York: CRC Press; 1995.
[57] Reddy YSN, Reddy JN. Linear and non-linear failure analysis of composite laminates with transverse shear. Comp Sci Technol 1992;44:227–55.
[58] Ericson K, Persson M, Carlsson L, Gustavsson A. On the prediction of the initiation of delamination in a $[0/90]_s$ laminate with a circular hole. J Compos Mate 1984;18:495–506.